IEEE Photonics Journal
An IEEE Photonics Society Publication

Open Access

Broadband Solar Spectral Conversion in Near-Infrared Quantum Cutting Ce^{3+}-Tb^{3+}/Yb^{3+} System for Improving Si Solar-Cell Performance

Volume 5, Number 2, April 2013

Pei Song
Chun Jiang

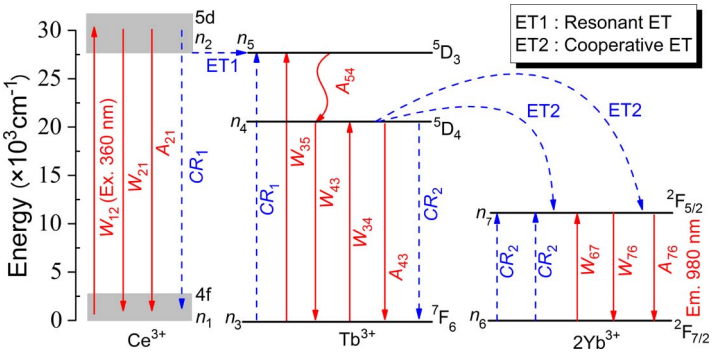

DOI: 10.1109/JPHOT.2013.2237897
1943-0655/$31.00 ©2013 IEEE

Broadband Solar Spectral Conversion in Near-Infrared Quantum Cutting Ce^{3+}-Tb^{3+}/Yb^{3+} System for Improving Si Solar-Cell Performance

Pei Song and Chun Jiang

State Key Laboratory of Advanced Optical Communication Systems and Networks, Shanghai Jiao Tong University, Shanghai 200240, China

DOI: 10.1109/JPHOT.2013.2237897
1943-0655/$31.00 ©2013 IEEE

Manuscript received November 29, 2012; revised December 23, 2012; accepted January 1, 2013. Date of publication January 4, 2013; date of current version March 6, 2013. This work was supported in part by the National Natural Science Foundation of China under Grant 61177056 and in part by Shanghai Pujiang Program. Corresponding author: C. Jiang (e-mail: cjiang@sjtu.edu.cn).

Abstract: In this paper, a framework for investigating and optimizing Ce^{3+}-Tb^{3+}/Yb^{3+} tripled-doped solar spectral downconverting layer is provided. We investigate broadband solar spectral downconversion in near-infrared (NIR) quantum cutting system of Ce^{3+}-Tb^{3+}/Yb^{3+} triple-doped YBO_3 employed by modeling and solving rate and power propagation equations of Ce^{3+}-Tb^{3+}/Yb^{3+}. For the optimized Ce^{3+}, Tb^{3+}, and Yb^{3+} concentrations and the thickness of doping layer, total power conversion efficiency of 176% and quantum conversion efficiency of 187% have been theoretically obtained. The total amount of NIR photon output may be increased to meet the purpose of potentially enabling a Si solar cell with a performance improvement. The paper will be also helpful to further investigate and design much more efficient rare-earth-multidoped system of broadband solar spectral conversion for further improving performances of Si solar cells.

Index Terms: Solar spectral downconversion (DC), photovoltaic (PV) cells, rare-earth (RE) material/devices, quantum cutting (QC), theoretical modeling.

1. Introduction

The main energy loss in crystalline Si (c-Si) solar cell for converting solar energy to electricity is related to the mismatch between the solar spectrum and the band-gap energy of c-Si solar cells. For photons with energy lower than the band gap, the energy cannot be absorbed, while for photons with energy larger than the band gap, the excess energy is lost by thermalization of hot charge carriers. The spectral mismatch limits photoelectric conversion efficiency of c-Si solar cells [1]. The solar spectral downconverting entities downconvert the wavelengths where the spectral response is low to wavelengths where the spectral response is high [2]–[5].

A promising method that helps the c-Si solar cell capture more energy is by solar spectral downconverter with rare-earth (RE) ion near-infrared quantum cutting (NIR QC), i.e., cutting a near-ultraviolet (UV) photon into two NIR photons that can be well absorbed by c-Si solar cells [6]. Effective spectral downconversion (DC) is obtained by combination of different RE ions in solar spectral downconverter and placing on the top of c-Si solar cells.

The NIR QC process has been reported in RE-codoped systems, which downconverts one UV or blue photon (300–500 nm) into two NIR photons that can be absorbed efficiently by c-Si solar cells. Incident solar photons with energy larger than twice the band gap of c-Si solar cells are absorbed

within the solar spectral downconverter and transformed into two or more lower energy photons employing by energy transfer (ET) between RE ions, which will reduce the energy loss related to thermalization of hot charge carriers and then improve photoelectric conversion efficiency of c-Si solar cells. NIR QC has been achieved firstly in $YPO_4 : Tb^{3+}$, Yb^{3+} where a visible photon is downconverted into two NIR photons through ET from Tb^{3+} ion to Yb^{3+} ion [7], and a cooperative dipole_dipole ET mechanism has been set up in Tb^{3+}-Yb^{3+} couple [8]. Recently, efficient QC in a variety of RE^{3+}-Yb^{3+} (RE = Yb, Tm, Ce, Nd, Pr, etc.) couples have been reported [9]–[12].

The NIR QC employing by RE^{3+}-Yb^{3+} couple would theoretically contribute the highest quantum conversion efficiency (QE) of 200%; however, there is a significant drawback. RE (RE = Yb, Tm, Nd, Pr, etc.) ions as absorption centers have narrow absorption linewidth and low absorption cross sections for UV or blue (300–500 nm) photons due to the forbidden nature of the 4f−4f transitions, resulting in lower direct excitation efficiency and weak NIR emission of Yb^{3+} ions, which makes it difficult to use the RE^{3+}-Yb^{3+} couple for practical applications because only a relatively small high energy part of the incident solar spectrum is used. Consequently, the actual NIR emission is still low, although the physics of the ET process allows for the efficient QC process. A promising NIR QC of Ce^{3}-Tb^{3+}/Yb^{3+} triple-doped system is developed, in which the 4f_5d luminescence of Ce^{3+} ion can be used to sensitize the Tb^{3+}-Yb^{3+} DC process and thus harvesting UV or blue photons and greatly improving NIR emission of Yb^{3+} ion at around 980 nm [13]–[15]. In virtue of NIR QC, total output power density and photon flux density for the modified solar spectrum are boosted relative to the solar spectrum incident directly at c-Si solar cells, which may improve the photoelectric conversion efficiency of c-Si solar cells.

The theoretical rate and power density equation models of RE-doped systems for fiber and waveguide amplifiers have been previously presented [16]–[23], while in this paper, we investigate NIR QC model of Ce^{3}-Tb^{3+}/Yb^{3+} triple-doped YBO_3 [24] by proposing the rate and power density propagation equations. The theoretical model is based on experimental values from literatures, and the power conversion efficiency (CE) and QE are calculated in MATLAB.

2. Modeling

2.1. Theoretical Model

A cooperative NIR QC process in the Tb^{3+}-Yb^{3+} dual-doped system was widely investigated where Tb^{3+} ion acts as the absorption center facilitating utilization of the UV or blue part of the incident solar spectrum and Yb^{3+} ion has a relatively simple electronic structure of two energy level manifolds: the $^2F_{7/2}$ ground state and $^2F_{5/2}$ excited state around 10 000 cm^{-1} in the NIR region and acts as an acceptor possessing a broadband emission (900–1100 nm), perfectly matching the optimal spectral response (1000 nm) of c-Si solar cells. In this process, one blue photon of Tb^{3+} ion from the absorption transition around 482 nm ($^7F_6 \rightarrow {}^5D_4$) is cut into two NIR photons of Yb^{3+} ions by the emission transition ($^2F_{5/2} \rightarrow {}^2F_{7/2}$) that can be expressed as $Tb^{3+}(^5D_4) + Yb^{3+}(^2F_{7/2}) \rightarrow Tb^{3+}(^7F_6) + 2Yb^{3+}(^2F_{5/2})$. Tb^{3+} ions as absorption centers have narrow absorption linewidth and low absorption cross sections for UV or blue photons due to the forbidden nature of the 4f_4f transitions, resulting in lower direct excitation efficiency and weak NIR emission of Yb^{3+} ions. The absorption spectra of Ce^{3+} ions generally consist of broadbands in the UV or blue regions due to the allowed 4f_5d transitions, and thus, the absorption linewidth and cross sections are wide and large, respectively. In addition, Ce^{3+} ions are efficient sensitizers, especially for Tb^{3+} ions. Therefore, Ce^{3+} ions can be used as sensitizing absorption centers to absorb the UV or blue part of the incident solar spectrum typically in the 300- to 500-nm range and efficiently transfer the excitation energy to the $^5D_3$ state of Tb^{3+} ions for the Tb^{3+}-Yb^{3+} NIR QC process. The energy difference between the lowest 5d excited level of Ce^{3+} ion and the $^2F_{5/2}$ level of Yb^{3+} ion is about 17548 cm^{-1}, which is 12.53 times as great as the highest vibration energy in YBO_3 ($\nu_{max} \approx 1400$ cm^{-1}) [14], [24]. It is difficult to bridge such a huge energy gap employing by assistance of photons, which suggests that, upon excitation of the Ce^{3+} ions, ET from Ce^{3+} ion to Yb^{3+} ion employed by Tb^{3+} ion dominates, whereas the direct ET from Ce^{3+} ion to Yb^{3+} ion can be negligible.

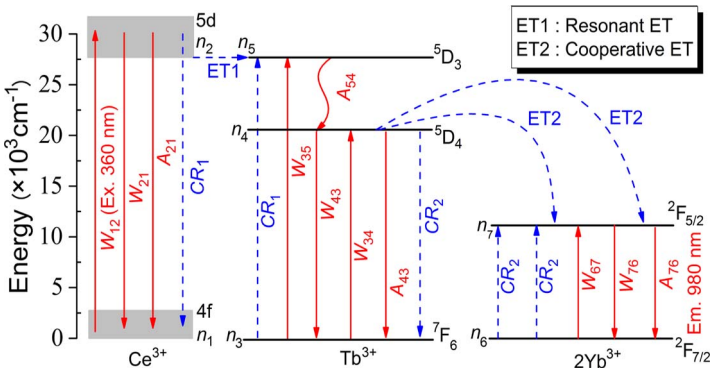

Fig. 1. Energy level scheme and the NIR QC mechanism of Ce^{3+}-Tb^{3+}/Yb^{3+} triple-doped system, showing the ET and DC processes.

The diagram of Ce^{3+}-Tb^{3+}/Yb^{3+} energy levels, the relevant absorption and emission transitions, spontaneous emission, and ET process between Ce^{3}-Tb^{3+}/Yb^{3+} are shown in Fig. 1. The QC system of Ce^{3}-Tb^{3+}/Yb^{3+} is equivalent to the system of pump-excitation transition where the population-rate equations show the QC process of Ce^{3}-Tb^{3+}/Yb^{3+} and the power density propagation equations show absorption and re-emission of input solar light during transmission within the spectral downconverting layer. The rate equations (1)–(3), (5), (7)–(9) and power density propagation equations (10), (11), (13) are ascribed to the Ce^{3+}-Tb^{3+}/Yb^{3+} triple-doped system, while a group of equations (4), (6), (8), (9), (12), and (13) are ascribed to the Tb^{3+}/Yb^{3+} dual-doped system as follows:

$$\frac{\partial n_1}{\partial t} = -W_{12}n_1 + W_{21}n_2 + A_{21}n_2 + C_{CR1}n_2n_4 \tag{1}$$

$$\frac{\partial n_2}{\partial t} = W_{12}n_1 - W_{21}n_2 - A_{21}n_2 - C_{CR1}n_2n_4 \tag{2}$$

$$\frac{\partial n_3}{\partial t} = -W_{35}n_3 + W_{43}n_4 + A_{43}n_4 + C_{CR2}n_4n_6 \tag{3}$$

$$\frac{\partial n_3}{\partial t} = -W_{34}n_3 + W_{43}n_4 + A_{43}n_4 + C_{CR2}n_4n_6 \tag{4}$$

$$\frac{\partial n_4}{\partial t} = A_{54}n_5 - A_{43}n_4 - W_{43}n_4 - C_{CR2}n_4n_6 - C_{CR1}n_2n_4 \tag{5}$$

$$\frac{\partial n_4}{\partial t} = W_{34}n_3 - A_{43}n_4 - W_{43}n_4 - C_{CR2}n_4n_6 \tag{6}$$

$$\frac{\partial n_5}{\partial t} = W_{35}n_3 + C_{CR1}n_2n_4 - A_{54}n_5 \tag{7}$$

$$\frac{\partial n_6}{\partial t} = -W_{67}n_6 + A_{76}n_7 + W_{76}n_7 - C_{CR2}n_4n_6 \tag{8}$$

$$\frac{\partial n_7}{\partial t} = W_{67}n_6 - A_{76}n_7 - W_{76}n_7 + C_{CR2}n_4n_6 \tag{9}$$

$$\frac{dP_{p1}(z,\lambda)}{dz} = [\sigma_{21}(\lambda)n_2 - \sigma_{12}(\lambda)n_1]P_{p1}(z,\lambda) - \alpha_p P_{p1}(z,\lambda) \tag{10}$$

$$\frac{dP_{p2}(z,\lambda)}{dz} = [\sigma_{43}(\lambda)n_4 - \sigma_{35}(\lambda)n_3]P_{p2}(z,\lambda) - \alpha_p P_{p2}(z,\lambda) \tag{11}$$

$$\frac{dP_{p2}(z,\lambda)}{dz} = [\sigma_{43}(\lambda)n_4 - \sigma_{34}(\lambda)n_3]P_{p2}(z,\lambda) - \alpha_p P_{p2}(z,\lambda) \quad (12)$$

$$\frac{dP_s(z,\lambda)}{dz} = [\sigma_{76}(\lambda)n_7 - \sigma_{67}(\lambda)n_6 - \alpha_s]P_s(z,\lambda) \quad (13)$$

where n_1(4f), n_2(5d), n_3($^7F_6$), n_4($^5D_4$), n_5($^5D_3$), n_6($^2F_{7/2}$), and n_7($^2F_{5/2}$) are the population densities of relevant energy levels of Ce^{3+}, Tb^{3+}, and Yb^{3+}, and n_i $(i,j = 1 \sim 7)$ is dependent of the thickness of doping layer z. A_{ij} $(i,j = 1 \sim 7)$ values are the respective spontaneous transition rates and nonradiation transition rates between energy levels i and j. $\sigma_{ij}(\lambda)(i,j = 1 \sim 7)$ is the absorption and emission cross section of the transition between the energy levels i and j. $P_p(z,\lambda)$ and $P_s(z,\lambda)$ are the corresponding input solar power density and output light power density. α_p and α_s are scattering losses and are assumed as frequency-independent constant for simplicity. C_{CR1} and C_{CR2} are the ET coefficient describing processes of CR1 and CR2, and are linearly increasing functions of Ce^{3+} and Tb^{3+} ion concentrations according to the theory of the resonant ET [25]

$$C_{CR1} = 8.00 \times 10^{-48}(N_{Ce3+} - 1.0 \times 10^{25}) + 2.0 \times 10^{-21} \quad (14)$$

$$C_{CR2} = 8.00 \times 10^{-48}(N_{Tb3+} - 1.0 \times 10^{25}) + 2.0 \times 10^{-21}. \quad (15)$$

W_{ij} $(i,j = 1 \sim 7)$ is the transition rate between energy levels i and j, and can be expressed as

$$W_{ij}(z,\lambda) = \frac{\sigma_{ij}(\lambda)P(z,\lambda)}{h\nu_{ij}A_{eff}} \quad (16)$$

where h is Plank's constant, v_{ij} is bandwidth, and A_{eff} is the effective cross-sectional area.

The total Ce^{3+}, Tb^{3+}, and Yb^{3+} concentrations N_{Ce3+}, N_{Tb3+}, and N_{Yb3+} are assumed to be constant within the whole Ce^{3+}-Tb^{3+}/Yb^{3+} triple-doped system that satisfy the conservation conditions

$$\sum_{i=1}^{2} n_i(z) - N_{Ce3+} = 0 \quad (17)$$

$$\sum_{i=3}^{5} n_i(z) - N_{Tb3+} = 0 \quad (18)$$

$$\sum_{i=6}^{7} n_i(z) - N_{Yb3+} = 0. \quad (19)$$

2.2. Theoretical Model Calculation

For the Ce^{3+}-Tb^{3+}/Yb^{3+} triple-doped and Tb^{3+}/Yb^{3+} dual-doped systems, considering an initial time-independent steady-state $\partial n_i/\partial t = 0$, the population rate equations are solved numerically employed by Newton's iterative method, while the power density propagation equations form a system of coupled differential equations, which are solved numerically employing by fourth-order Runge–Kutta methods with some boundary conditions $P_{p1}(z = 0, v) = P^*_{p01}$, $P_{p2}(z = 0, v) = P^*_{p02}$, and $P_s(z = 0, v) = P_{s0}$. For our simulation, we select YBO_3 as NIR QC host materials. The spectroscopic parameters used in calculation [24] are listed in Table 1.

We choose 360 and 482 nm as center excitation wavelength of Ce^{3+} and Tb^{3+} ions, respectively, and 980 nm as emission wavelength of Yb^{3+} ion. In order to calculate the effective absorption of the input solar spectrum in the system accurately, Ce^{3+} and Tb^{3+} absorption linewidths at around 360 and 482 nm should be taken into account. Incident solar spectrum is normalized for the case of complete absorption of incident solar emission in the spectral region corresponding to 360 and

TABLE 1

Parameters used in MATLAB calculation

Scattering loss coefficient (α_p, α_s)	0.1 db/m
Ce^{3+} 360 nm absorption cross section (σ_{12})	9.9×10^{-24} m^2
Ce^{3+} 360 nm radiation cross section (σ_{21})	5.0×10^{-24} m^2
Ce^{3+} spontaneous emission rate (A_{21})	51000 s^{-1}
Tb^{3+} 377 nm absorption cross section (σ_{35})	1.38×10^{-26} m^2
Tb^{3+} 482 nm absorption cross section (σ_{34})	1.24×10^{-26} m^2
Tb^{3+} 482 nm radiation cross section (σ_{43})	3.25×10^{-26} m^2
Tb^{3+} spontaneous emission rate (A_{54})	48030 s^{-1}
Tb^{3+} spontaneous emission rate (A_{43})	150.19 s^{-1}
Yb^{3+} 980 nm absorption cross section (σ_{67})	1.32×10^{-24} m^2
Yb^{3+} 980 nm radiation cross section (σ_{76})	1.40×10^{-24} m^2
Yb^{3+} spontaneous emission rate (A_{76})	10 s^{-1}
Initial effective pump power density (P_{p01}^{*})	0.205 W/m^2
Initial effective pump power density (P_{p02}^{*})	0.269 W/m^2
Initial signal power density (P_{s0})	0.299 W/m^2

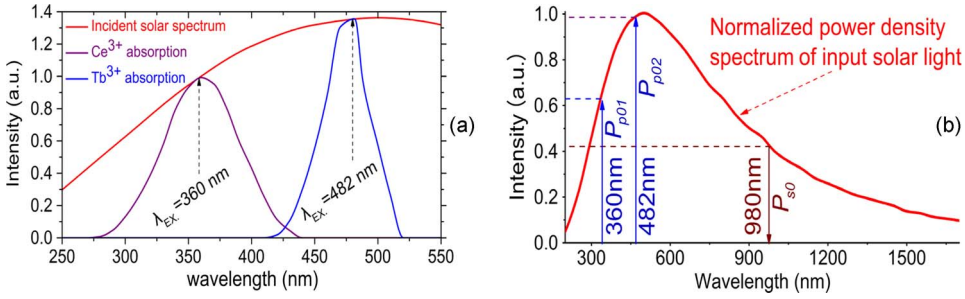

Fig. 2. (a) Ce^{3+} and Tb^{3+} absorption spectrum and incident solar spectrum for calculation of Γ_i. (b) Normalized power density spectrum of incident solar light, and the relation of $P_{p01} : P_{p02} : P_{s0}$ is 0.62 : 0.98 : 0.42.

482 nm absorption band of Ce^{3+} and Tb^{3+}. Overlap coefficient $\Gamma_i (i = 1, 2)$ of Ce^{3+} and Tb^{3+} absorption spectrum and incident solar spectrum is defined as

$$\Gamma_i = \frac{\int_\lambda I_{ab.}(\lambda) d\lambda}{\int_\lambda I_{so.}(\lambda) d\lambda} \tag{20}$$

where $I_{ab.}(\lambda)$ and $I_{so.}(\lambda)$ are Ce^{3+} (or Tb^{3+}) absorption peak near 360-nm (or 482-nm) center excitation wavelength and solar spectrum near 360-nm (or 482-nm) center wavelength, respectively.

Γ_1 and Γ_2 are calculated as 41% and 38%, which means that such proportion of incident solar energy can be absorbed effectively in the system, as shown in Fig. 2(a). For simulation, we set 500 mW/m^2 as initial solar power density incident at 360 nm, and initial effective solar power density P_{p10} of 205 W/m^2 incident at 360 nm and P_{p20} of 268.7 W/m^2 incident at 482 nm are calculated via $P_{p10} * \Gamma_1$ and $P_{p20} * \Gamma_2$, respectively. We also calculate initial 980-nm output light power density P_{s0} of 298.9 mW/m^2 employing by the spectrum of the normalized solar power density [26], as shown in Fig. 2(b). Initial N_{Ce3+}, N_{Tb3+}, N_{Yb3+}, and z are set to be 1.0×10^{25}, 1.0×10^{25}, 1.0×10^{25} ions/m^3, and 5.0×10^{-3} m, respectively. Effective absorption of input solar spectrum in the system we analyzed above is taken into account in MATLAB simulation.

CE (η) and QE (q) for the Ce^3-Tb^{3+}/Yb^{3+} triple-doped and Tb^{3+}/Yb^{3+} dual-doped systems are defined in order to exhibit the effect of spectral DC

$$\eta(z,\lambda) = \frac{\int_{\lambda=200}^{1500} P_s(z,\lambda)d\lambda}{\int_{\lambda=200}^{1500} P_{in}(z,\lambda)d\lambda} \tag{21}$$

$$q(z,\lambda) = \frac{\int_{\lambda=200}^{1500} N_s(z,\lambda)d\lambda}{\int_{\lambda=200}^{1500} N_{in}(z,\lambda)d\lambda}. \tag{22}$$

Total CE (η^*) and QE (q^*) for the triple- and dual-doped system based on total solar spectrum in the range of 200–1500 nm are defined as

$$\eta^*(z,\lambda) = \frac{\int_{\lambda=200}^{1500} P_{out}(z,\lambda)d\lambda}{\int_{\lambda=200}^{1500} P_{in}(z,\lambda)d\lambda} = \frac{\int_{\lambda=200}^{1500} [P_{in}(z,\lambda) + P_s(z,\lambda) - P_{ab}(z,\lambda)]d\lambda}{\int_{\lambda=200}^{1500} P_{in}(z,\lambda)d\lambda} \tag{23}$$

$$q^*(z,\lambda) = \frac{\int_{\lambda=200}^{1500} N_{out}(z,\lambda)d\lambda}{\int_{\lambda=200}^{1500} N_{in}(z,\lambda)d\lambda} = \frac{\int_{\lambda=200}^{1500} [N_{in}(z,\lambda) + N_s(z,\lambda) - N_{ab}(z,\lambda)]d\lambda}{\int_{\lambda=200}^{1500} N_{in}(z,\lambda)d\lambda} \tag{24}$$

where $P_{out}(\lambda)$ and $N_{out}(\lambda)$ are the spectrum of total output power density and the spectrum of total output photon flux density, respectively. $P_{in}(\lambda)$, $P_{ab}(\lambda)$, and $P_s(\lambda)$ are the spectrum of input solar power density, Ce^{3+} and Tb^{3+} absorption power density at 360 and 482 nm, and Yb^{3+} output power density at around 980 nm, respectively. $N_{in}(\lambda)$, $N_{ab}(\lambda)$, and $N_s(\lambda)$ are the respective spectrum of photon flux density.

2.3. Modeling Results and Discussion

Concentration effects of Ce^{3+}, Tb^{3+}, and Yb^{3+} ions on CE and QE are shown in Figs. 3–5, in the analysis; z is fixed at 5.0×10^{-3} m. As shown in Fig. 3, as N_{Ce3+} increases from 1.0×10^{25} ions/m^3 to 4.0×10^{25} ions/m^3, CE and QE decrease slightly from 36.93% to 36.89% and from 46.23% to 46.15%, respectively. As shown in Figs. 4 and 5, CE and QE increase clearly with increased N_{Tb3+} and N_{Yb3+} from 0 to 3.0×10^{25} ions/m^3. Variations of CE and QE are less sensitive to a variation of N_{Ce_3+} than a variation of N_{Tb3+} and N_{Yb3+} in the Ce^{3+}-Tb^{3+}/Yb^{3+} triple-doped system; moreover, variations of CE and QE are less sensitive to a variation of N_{Tb3+} than a variation of N_{Tb3+} in the Tb^{3+}/Yb^{3+} dual-doped system. In Figs. 4 and 5, it can be observed that Tb^{3+} luminescence is highly enhanced, where CE and QE are higher in the Ce^{3+}-Tb^{3+}/Yb^{3+} triple-doped system than those in

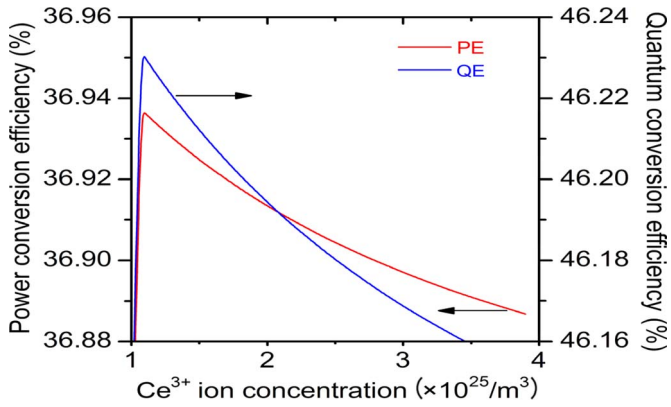

Fig. 3. Here, z is fixed at 5.0×10^{-3} m, N_{Tb3+}, N_{Yb3+} are fixed at 6.0×10^{25} and 8.0×10^{25} ions/m^3, respectively. Variation of CE and QE with N_{Ce3+} from 1.0×10^{25} ions/m^3 to 4.0×10^{25} ions/m^3.

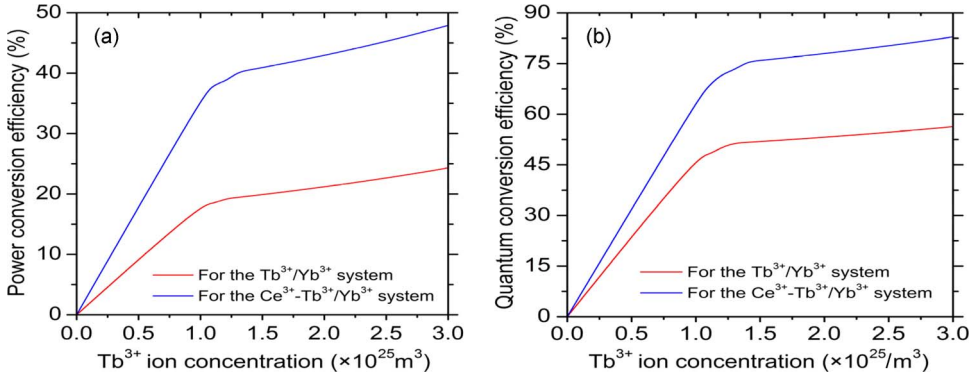

Fig. 4. CE and QE for the Ce^{3+}-Tb^{3+}/Yb^{3+} triple-doped system compared with the Tb^{3+}/Yb^{3+} dual-doped system. Here, z is fixed at 5.0×10^{-3} m, N_{Ce3+}, N_{Yb3+} are fixed at 1.0×10^{25} and $8.0 \times 10_{25}$ ions/m^3, respectively. (a) Variation of CE and QE with N_{Tb3+} from 0 to 3.0×10^{25} ions/m^3. (b) Variation of CE and QE with N_{Tb3+} from 0 to 3.0×10^{25} ions/m^3.

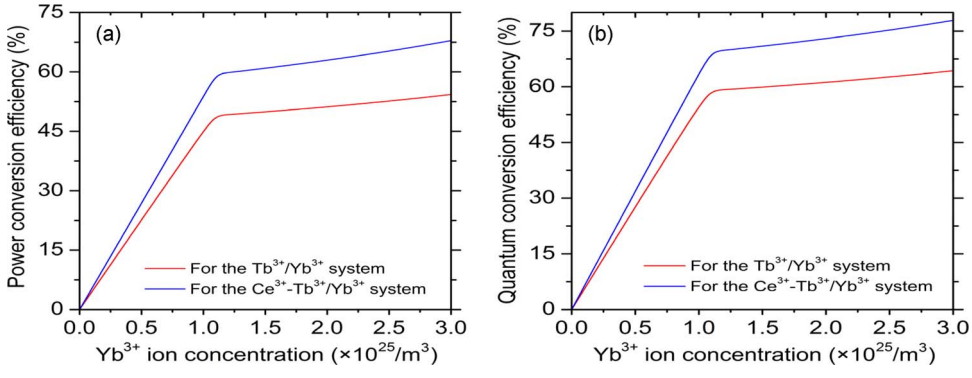

Fig. 5. CE and QE for the Ce^{3+}-Tb^{3+}/Yb^{3+} triple-doped system compared with the Tb^{3+}/Yb^{3+} dual-doped system. Here, z is fixed at 5.0×10^{-3} m, N_{Ce3+}, N_{Tb3+} are fixed at 1.0×10^{25} and 6.0×10^{25} ions/m^3, respectively. (a) Variation of CE and QE with N_{Yb3+} from 0 to 3.0×10^{25} ions/m^3. (b) Variation of CE and QE with N_{Yb3+} from 0 to 3.0×10^{25} ions/m^3.

Tb^{3+}/Yb^{3+} dual-doped system. It is indicated that optimal CE and QE should be much better for lower N_{Ce3+}, higher N_{Tb3+}, and N_{Yb3+} in a definite range ascribed to the concentration quenching of Ce^{3+}, Tb^{3+}, and Yb^{3+}. In our simulation, CE and QE reach maxima only when N_{Ce3+}, N_{Tb3+}, and N_{Yb3+} reach the optimal values of 1.0×10^{25}, 6.3×10^{25}, and 8.7×10^{25} ions/m^3, respectively.

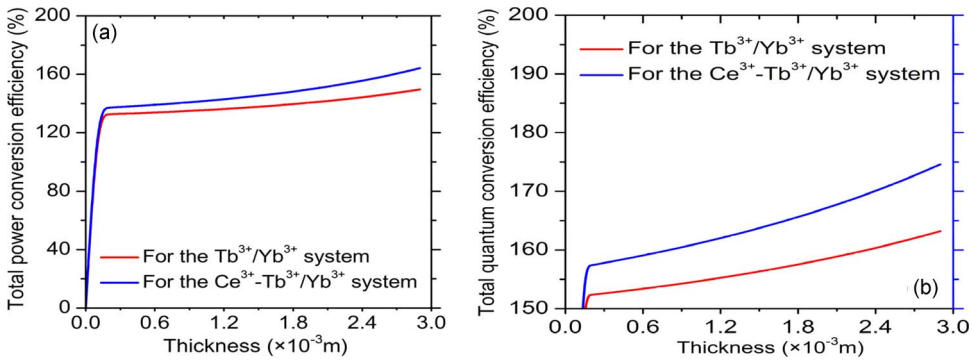

Fig. 6. Total CE and QE for the Ce^{3+}-Tb^{3+}/Yb^{3+} triple-doped system compared with the Tb^{3+}/Yb^{3+} dual-doped system. Here, N_{Ce3+}, N_{Tb3+}, N_{Yb3+} are fixed at 1.0×10^{25}, 6.0×10^{25} and 8.0×10^{25} ions/m^3, respectively. (a) Variation of total CE and QE with z from 0 to 3.0×10^{-3} m. (b) Variation of total CE and QE with z from 0 to 3.0×10^{-3} m.

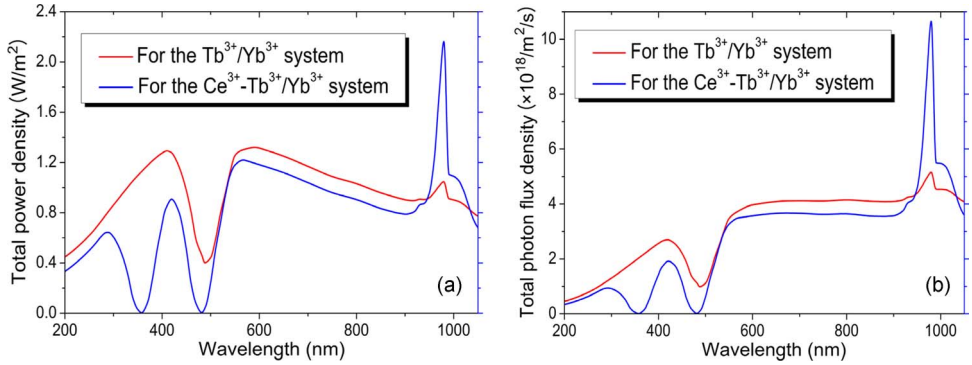

Fig. 7. Modified spectrum for the Ce^{3+}-Tb^{3+}/Yb^{3+} triple-doped system compared with the Tb^{3+}/Yb^{3+} dual-doped system. (a) Variation of $P_{out}(\lambda)$ with wavelength. (b) Variation of $N_{out}(\lambda)$ with wavelength.

The dependence of total CE and QE on z is shown in Fig. 6, and in the analysis, N_{Ce3+}, N_{Tb3+}, and N_{Yb3+} are fixed at 1.0×10^{25}, 6.0×10^{25}, and 8.0×10^{25} ions/m^3, respectively. Enhancement of both total CE and QE with increase in z is exhibited. As z increases from 0 to 3.0×10^{-3} m, total CE and QE increase clearly; moreover, total CE and QE are overall higher in the Ce^{3+}-Tb^{3+}/Yb^{3+} triple-doped system than those in the Tb^{3+}/Yb^{3+} dual-doped system. It should be pointed out that total CE and QE will no longer increase when z exceeds the optimal value, ascribed to absorption losses and side scatting losses within the solar spectral downconverting layer [27]. In our simulation, we obtain the maximum total CE of 176% and total QE of 187% for $z = 5.0 \times 10^{-3}$ m, when optimal N_{Ce3+}, N_{Tb3+}, and N_{Yb3+} are 1.0×10^{25}, 6.3×10^{25}, and 8.7×10^{25} ions/m^3, respectively. It is shown that the maximum CE and QE in our simulation are in good agreement with experimental results [24], verifying the feasibility and effectiveness of our simulated QC system of Ce^{3+}-Tb^{3+}/Yb^{3+}. We can calculate accurately the efficiency of solar spectral DC and acquire optimal system parameters, i.e., dopant concentrations and thickness of doping layers.

$P_{out}(\lambda)$ and $N_{out}(\lambda)$ are shown in Fig. 7. The obvious absorption peak at around 360 and 482 nm and emission peak at around 980 nm are observed in the Ce^{3+}-Tb^{3+}/Yb^{3+} triple-doped system. The spectrum curves directly indicate the effective processes of QC in the Ce^{3+}-Tb^{3+}/Yb^{3+} triple-doped system. Fig. 7 illustrates that in virtue of NIR QC, $P_{out}(\lambda)$, and $N_{out}(\lambda)$ at around 980 nm form the modified solar spectrum are boosted relative to the normalized solar spectrum directly incident at c-Si solar cells, and c-Si solar cells may obtain more energies and photons number from the modified solar spectrum than not-modified solar spectrum; therefore, the total amount of NIR photon

output increasing to meet the purpose of improving photoelectric conversion efficiency of c-Si solar cells can be expected.

3. Conclusion

In conclusion, the ET mechanism of NIR QC for Ce^{3+}-Tb^{3+}/Yb^{3+} based on the rate and power density propagation equations have been investigated, and the NIR QC model has been solved numerically employing by MATLAB. Variation of CE and QE with the thickness of doping layers and dopant concentrations has been investigated, and CE of 176% and QE of 187% under optimized Ce^{3+}, Tb^{3+}, and Yb^{3+} concentrations have been obtained.

In this paper, we have set up an effective theoretical model for simulating Ce^{3+}-Tb^{3+}/Yb^{3+} triple-doped system, accurately calculated CE and QE of solar spectral DC, and acquired optimal system parameters. The models and techniques that we have proposed in this paper will be helpful to further investigate and design much more efficient RE-multidoped NIR QC system for further improving performances of Si solar cells.

References

[1] T. Trupke, M. A. Green, and P. Würfel, "Improving solar cell efficiencies by down-conversion of high-energy photons," *J. Appl. Phys.*, vol. 92, no. 3, pp. 1647–1668, Aug. 2002.

[2] W. G. J. H. M. van Sark, "Enhancement of solar cell performance by employing planar spectral converters," *Appl. Phys. Lett.*, vol. 87, no. 15, pp. 151117-1–151117-3, Oct. 2005.

[3] W. G. J. H. M. van Sark, A. Meijerink, R. E. I. Schropp, J. A. M. van Roosmalen, and E. H. Lysen, "Enhancing solar cell efficiency by using spectral converters," *Sol. Energy Mater. Sol. Cells*, vol. 87, no. 1–4, pp. 395–409, May 2005.

[4] W. G. J. H. M. van Sark, "Simulating performance of solar cells with spectral downshifting layers," *Thin Solid Films*, vol. 516, no. 20, pp. 6808–6812, Aug. 2008.

[5] W. G. J. H. M. van Sark, A. Meijerink, R. E. I. Schropp, J. A. M. van Roosmalen, and E. H. Lysen, "Modeling improvement of spectral response of solar cells by deployment of spectral converters containing semiconductor nanocrystals," *Semiconductors*, vol. 38, no. 8, pp. 962–969, Aug. 2004.

[6] R. T. Wegh, H. Donker, K. D. Oskam, and A. Meijerink, "Visible quantum cutting in LiGdF4:Eu^{3+} through downconversion," *Science*, vol. 283, no. 5402, pp. 663–666, Jan. 1999.

[7] P. Vergeer, T. J. H. Vlugt, M. H. F. Kox, M. I. Den Hertog, J. P. J. M. Van der Eerden, and A. Meijerink, "Quantum cutting by cooperative energy transfer in Yb_xY_{1-x} PO_4 : Tb^{3+}," *Phys. Rev. B, Condens. Matter*, vol. 71, no. 1, pp. 014119-1–014119-11, Jan. 2005.

[8] B. S. Richards, "Luminescent layers for enhanced silicon solar cell performance: Down-conversion," *Sol. Energy Mater. Sol. Cells*, vol. 90, no. 9, pp. 1189–1207, May 2006.

[9] X. F. Liu, Y. Teng, Y. X. Zhuang, J. H. Xie, Y. B. Qiao, G. P. Dong, D. P. Chen, and J. R. Qiu, "Broadband conversion of visible light to near-infrared emission by Ce^{3+},Yb^{3+}-codoped yttrium aluminum garnet," *Opt. Lett.*, vol. 34, no. 22, pp. 3565–3567, Nov. 2009.

[10] Y. Teng, J. J. Zhou, X. F. Liu, S. Ye, and J. R. Qiu, "Efficient broadband near-infrared quantum cutting for solar cells," *Opt. Exp.*, vol. 18, no. 9, pp. 9671–9676, Apr. 2010.

[11] Q. Y. Zhang, G. F. Yang, and Z. H. Jiang, "Cooperative downconversion in $GdAl_3(BO_3)_4$: RE^{3+},Yb^{3+} (RE = Pr, Tb, and Tm)," *Appl. Phys. Lett.*, vol. 91, no. 5, pp. 051903-1–051903-3, Jul. 2007.

[12] X. Huang, S. Han, W. Huang, and X. Liu, "Enhancing solar cell efficiency: The search for luminescent materials as spectral converters," *Chem. Soc. Rev.*, vol. 42, no. 1, pp. 173–201, Jan. 2013.

[13] X. Y. Huang, D. C. Yu, and Q. Y. Zhang, "Enhanced near-infrared quantum cutting in $GdBO_3$: Tb^{3+},Yb^{3+} phosphors byCe^{3+} codoping," *J. Appl. Phys.*, vol. 106, no. 11, pp. 113521-1–113521-6, Dec. 2009.

[14] Q. H. Zhang, J. Wang, G. G. Zhang, and Q. Su, "UV photon harvesting and enhanced near-infrared emission in novel quantum cutting Ca_2BO_3Cl : Ce^{3+},Tb^{3+},Yb^{3+} phosphor," *J. Mater. Chem.*, vol. 19, no. 38, pp. 7088–7092, Jul. 2009.

[15] G. X. Liu and J. X. Meng, "Preparation and near-infrared quantum cutting luminescent properties of Na_2SrSiO_4 : Ce^{3+},Tb^{3+},Yb^{3+} phosphor," *Chin. J. Spectrosc. Lab.*, vol. 28, no. 5, pp. 2179–2182, Sep. 2011.

[16] M. Federighi and F. Di Pasquale, "The effect of pair-induced energy transfer on the performance of silica waveguide amplifiers with high Er^{3+}/Yb^{3+} concentrations," *IEEE Photon. Technol. Lett.*, vol. 7, no. 3, pp. 303–305, Mar. 1995.

[17] E. Yahel and A. Hardy, "Modeling high-power Er^{3+}-Yb^{3+} codoped fiber lasers," *J. Lightwave Technol.*, vol. 21, no. 9, pp. 2044–2052, Sep. 2003.

[18] M. Karasek, "Optimum design of Er^{3+}-Yb^{3+} codoped fibers for large-signal high-pump-power applications," *IEEE J. Quantum Electron.*, vol. 33, no. 10, pp. 1699–1705, Oct. 1997.

[19] C. Jiang, "Numerical simulation of 980 nm-LD-pumped Yb^{3+}-Er^{3+}-Tm^{3+}-codoped fiber amplifier for 1500 nm and 1600 nm bands," *Adv. OptoElectron.*, vol. 2009, pp. 278105-1–278105-8, Jun. 2009.

[20] L. Jin, D. Ma, Y. Q. Ding, and C. Jiang, "Theoretical analysis of gain characteristics of Er^{3+}-Tm^{3+}-codoped tellurite fiber amplifier," *IEEE Photon. Technol. Lett.*, vol. 18, no. 3, pp. 460–462, Feb. 2006.

[21] W. H. Xu, Y. M. Lin, and C. Jiang, "Er^{3+}-Tm^{3+}-codoped tellurite fiber amplifiers for WDM systems: A theoretical analysis of BER and bandwidth," *IEEE J. Quantum Electron.*, vol. 45, no. 1, pp. 3–9, Jan. 2009.

[22] C. Jiang and W. B. Xu, "Theoretical model of Yb^{3+}-Er^{3+}-Tm^{3+}-codoped system for white light generation," *J. Display Technol.*, vol. 5, no. 8, pp. 312–318, Aug. 2009.
[23] C. Jiang, "Modeling a broadband Bismuth-doped fiber amplifier," *IEEE J. Sel. Topics Quantum Electron.*, vol. 15, no. 1, pp. 79–84, Jan. 2009.
[24] X. Y. Huang, "Downconversion luminescence properties of rare-earth ions doped luminescent materials," Ph.D. dissertation, MOE Key Lab Spec. Funct. Mater. Inst. Opt. Commun. Mater., South China Univ. Technol., Guangzhou, China, 2011.
[25] M. Federighi and F. Di Pasquale, "The effect of pair-induced energy transfer on the performance of silica waveguide amplifiers with high Er^{3+}/Yb^{3+} concentration," *IEEE Photon. Technol. Lett.*, vol. 7, no. 3, pp. 303–305, Mar. 1995.
[26] B. S. Richards, "Enhancing the performance of silicon solar cells via the application of passive luminescence conversion layers," *Sol. Energy Mater. Sol. Cells*, vol. 90, no. 15, pp. 2329–2337, Sep. 2006.
[27] J. J. Zhou, Y. Teng, S. Ye, G. Lin, and J. R. Qiu, "A discussion on spectral modification from visible to near-infrared based on energy transfer for silicon solar cells," *Opt. Mater.*, vol. 34, no. 5, pp. 901–905, Mar. 2012.